Acute Middle East Respiratory Syndrome Coronavirus: Temporal Lung Changes Observed on the Chest Radiographs of 55 Patients

Karuna M. Das[1,2]
Edward Y. Lee[3,4]
Suhayla E. Al Jawder[5]
Mushira A. Enani[6]
Rajvir Singh[7]
Leila Skakni[8]
Nizar Al-Nakshabandi[1,9]
Khalid AlDossari[1]
Sven G. Larsson[1]

Keywords: chest radiographic score, chest radiographs, Middle East respiratory syndrome coronavirus (MERS-CoV), mortality, radiographic deterioration pattern

DOI:10.2214/AJR.15.14445

Received January 20, 2015; accepted after revision March 16, 2015.

[1]Department of Medical Imaging, King Fahad Medical City, Riyadh 11525, KSA. Address correspondence to K. M. Das (daskmoy@gmail.com).

[2]Department of Radiology, College of Medicine and Health Sciences, United Arab Emirates University, Al-Ain, UAE.

[3]Department of Radiology, Boston Children's Hospital and Harvard Medical School, Boston, MA.

[4]Department of Medicine, Pulmonary Division, Boston Children's Hospital and Harvard Medical School, Boston, MA.

[5]Department of Pulmonary & Sleep Medicine, King Fahad Medical City, Riyadh, KSA.

[6]Department of Medicine, Infectious Disease Division, King Fahad Medical City, Riyadh, KSA.

[7]Department of Cardiology, Hamad Medical Corporation, Doha, Qatar.

[8]Department of Virology, King Fahad Medical City, Riyadh, KSA.

[9]Department of Radiology, College of Medicine, King Saud University, Riyadh, KSA.

This is an ahead-of-print version of the article; the final version will appear in the September 2015 issue of the *AJR*.

WEB
This is a web exclusive article.

AJR 2015; 205:W1–W8

0361–803X/15/2053–W1

OBJECTIVE. The objective of our study was to describe lung changes on serial chest radiographs from patients infected with the acute Middle East respiratory syndrome coronavirus (MERS-CoV) and to compare the chest radiographic findings and final outcomes with those of health care workers (HCWs) infected with the same virus. Chest radiographic scores and comorbidities were also examined as indicators of a fatal outcome to determine their potential prognostic value.

MATERIALS AND METHODS. Chest radiographs of 33 patients and 22 HCWs infected with MERS-CoV were examined for radiologic features indicative of disease and for evidence of radiographic deterioration and progression. Chest radiographic scores were estimated after dividing each lung into three zones. The scores (1 [mild] to 4 [severe]) for all six zones per chest radiographic examination were summed to provide a cumulative chest radiographic score (range, 0–24). Serial radiographs were also examined to assess for radiographic deterioration and progression from type 1 (mild) to type 4 (severe) disease. Multivariate logistic regression analysis, Kaplan-Meier survival curve analysis, and the Mann-Whitney U test were used to compare data of deceased patients with those of individuals who recovered to identify prognostic radiographic features.

RESULTS. Ground-glass opacity was the most common abnormality (66%) followed by consolidation (18%). Overall mortality was 35% (19/55). Mortality was higher in the patient group (55%, 18/33) than in the HCW group (5%, 1/22). The mean chest radiographic score for deceased patients was significantly higher than that for those who recovered (13 ± 2.6 [SD] vs 5.8 ± 5.6, respectively; $p = 0.001$); in addition, higher rates of pneumothorax (deceased patients vs patients who recovered, 47% vs 0%; $p = 0.001$), pleural effusion (63% vs 14%; $p = 0.001$), and type 4 radiographic progression (63% vs 6%; $p = 0.001$) were seen in the deceased patients compared with those who recovered. Univariate and logistic regression analyses identified the chest radiographic score as an independent predictor of mortality (odds ratio [OR], 1.38; 95% CI, 1.07–1.77; $p = 0.01$). The number of comorbidities in the patient group ($n = 33$) was significantly higher than that in the HCW group ($n = 22$) (mean number of comorbidities, 1.90 ± 1.27 vs 0.17 ± 0.65, respectively; $p = 0.001$). The Kaplan-Meier analysis revealed a median survival time of 15 days (95% CI, 4–26 days).

CONCLUSION. Ground-glass opacity in a peripheral location was the most common abnormality noted on chest radiographs. A higher chest radiographic score coupled with a high number of medical comorbidities was associated with a poor prognosis and higher mortality in those infected with MERS-CoV. Younger HCWs with few or no comorbidities had a higher survival rate.

Outbreaks of acute infection by the Middle East respiratory syndrome coronavirus (MERS-CoV) were recently reported by health authorities in Riyadh, Saudi Arabia [1]. The first case was identified in September 2012. As of December 17, 2014, the number of MERS-CoV-infected patients had increased to 821, with 355 recorded deaths [2]. Most patients with MERS-CoV infection present with nonspecific clinical symptoms such as fever, cough, and shortness of breath [3, 4].

One of the recent studies reported unilateral and bilateral lung abnormalities ranging from subtle to extensive on chest radiographs in 87% of 47 patients with MERS-CoV [5]. However, the report did not specifically examine the type and extent of the pulmonary

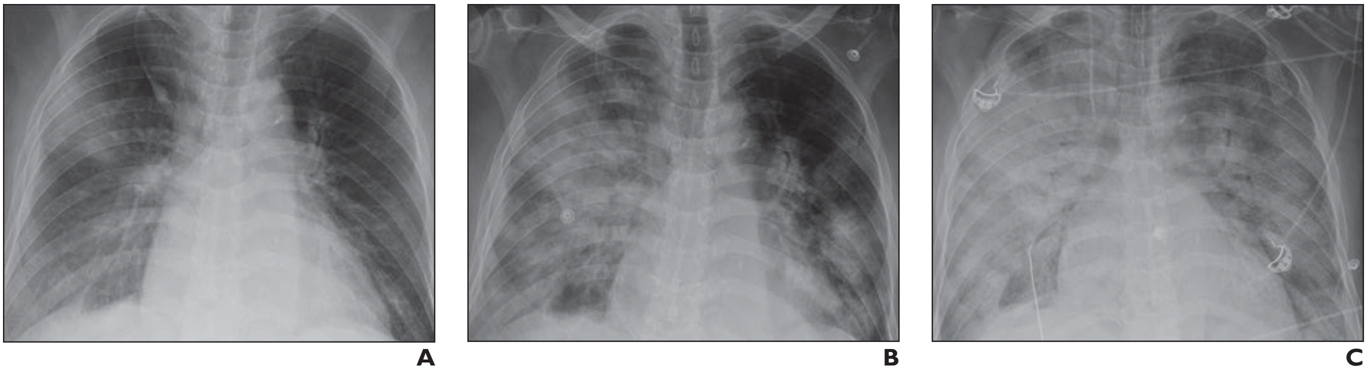

Fig. 1—69-year-old man with Middle East respiratory syndrome coronavirus. Serial chest radiographs show type 4 pattern of progression.
A, Frontal chest radiograph obtained at first presentation shows unilateral peripheral focal consolidation in right upper zone and ground-glass opacity in right lower zone; chest radiographic score is 2.
B, Follow-up frontal chest radiograph obtained on day 5 shows multifocal bilateral airspace opacities in both lungs, indicating disease progression; chest radiographic score of 9.5.
C, Subsequent follow-up chest radiograph obtained on day 8 shows moderate left-sided pleural effusion, indicating further deterioration; chest radiographic score is 15.5. Patient died on 8th day after admission.

abnormalities or their relationship to the final outcome. The findings presented herein expand on this previous study and show that a higher chest radiographic score (i.e., more extensive lung abnormalities) is associated with a poor prognosis and a higher mortality rate in patients infected with MERS-CoV.

At our institutions, we observed signs of MERS-CoV infection on a number of chest radiographs. Chest radiography plays a crucial role in the early diagnosis of infection and monitoring of disease progression during medical treatment [6]. Therefore, the aim of the current study was to examine serial chest radiographs of patients infected with MERS-CoV to identify pathologic changes in the lungs that are associated with the final outcome. The chest radiographic findings and final outcomes of patients were compared with those of health care workers (HCWs) infected with the same virus.

Materials and Methods

Subjects

This retrospective study was approved by the institutional review board, and the requirement for informed consent was waived. Fifty-five subjects (39 females and 16 males; mean age, 46.9 years; range, 12–85 years) were enrolled in the study, and 581 (mean, 10.6 ± 9.8; range, 1–47) chest radiographic examinations were obtained. The initial chest radiographic study was obtained 2.5 ± 1 days (mean ± SD; range, 1–5 days) after the onset of symptoms. The 55 subjects were divided into two different cohorts: patients (n = 33, 21 females and 12 males; mean age, 54 ± 16 years; range, 12–85 years) with epidemiologic links to confirmed MERS-CoV cases and HCWs (n = 22, 18 women and four men; mean age, 34 ± 7 years; range, 26–56 years) with a history of direct contact with MERS-CoV-infected patients admitted to the hospital. All subjects were diagnosed with MERS-CoV infection between April 7, 2014, and August 28, 2014. All subjects received appropriate supportive care: oral ribavirin (dose based on the calculated creatinine clearance rate) and subcutaneous pegylated interferon-α2a (180 μg/wk for 2 weeks).

The CT findings of 15 of the 55 subjects were published in an article in the April 2015 issue of the *AJR* [7]. The current study presents a detailed analysis of chest radiographic findings of the 55 subjects. Data from the patient and HCW groups were compared. MERS-CoV was diagnosed according to World Health Organization criteria: A confirmed case was defined as a suspected case that was positive for MERS-CoV by real-time reverse transcription polymerase chain reaction (RT-PCR) [6].

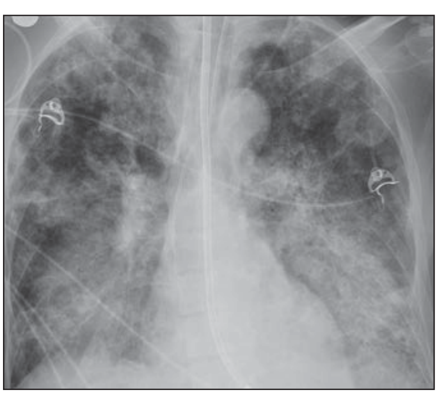

Fig. 2—44-year-old man with end-stage renal disease who developed Middle East respiratory syndrome coronavirus. Frontal chest radiograph obtained at day 6 shows bilateral multifocal patchy airspace disease with predominant perihilar distribution and multiple areas of cavitation; chest radiographic score is 13.

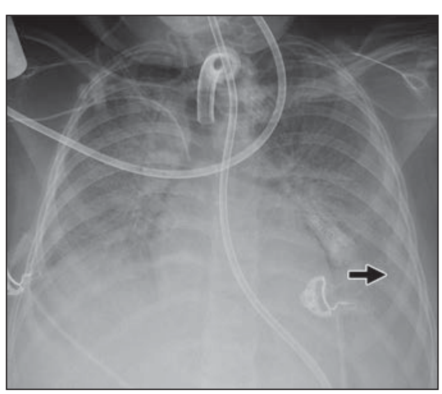

Fig. 3—12-year-old boy with preexisting craniopharyngioma who developed Middle East respiratory syndrome coronavirus. Frontal chest radiograph obtained on day 6 shows bilateral diffuse hazy pulmonary ground-glass opacification and moderate left-sided pleural effusion (*arrow*); chest radiographic score is 15. Patient died 8 days after initial presentation.

Chest Radiography and Evaluation

All chest radiographs obtained on admission to the department of emergency medicine and subsequent radiographs obtained during the course of treatment were included in the study. Throughout the study period, routine posteroanterior chest radiographs were obtained using digital radiography, and a lateral view was obtained if requested (n = 21). Anteroposterior views were obtained at the bedside in ICU patients and in patients who were not able to stand. Radiographs were obtained using portable computed radiographic equipment (Mobilett Plus, Siemens Healthcare) and standard techniques [8]. Patients in a serious condition underwent follow-up radiography daily while in the hospital. Radiographs were obtained every other day during the recovery period.

Interpretation of Chest Radiographs

Serial frontal chest radiographs obtained at initial presentation and during treatment were retrospectively reviewed and a consensus opinion was provided by three radiologists, none of whom was aware of the clinical progress of the subjects. The radiologists involved in the review process had 8, 20, and 40 years' experience with chest radiography reporting. The radiographs were viewed on a dedicated radiology PACS workstation (Centricity 2.1.2.1, GE Healthcare). The radiographs were examined for the presence of ground-glass opacity, consolidation, cavitation, pneumothorax, and pleural effusion, and findings were recorded using the Fleischner Society nomenclature [9]. In addition, the presence of multiple irregular linear airspace opacities was recorded [10].

The distribution of disease was rated as central if the abnormality predominantly involved the medial half of the lung and as peripheral if it predominantly involved the lateral half of the lung. Lung findings were recorded as unifocal or multifocal depending on whether the lung parenchyma was involved. Each lung was divided into three zones, and each zone was evaluated in terms of involvement [8]. The development of MERS-CoV lesions within each lung zone was assigned a score ranging from 0 (normal) to 4 (complete involvement of one zone); a score of 24 indicated complete involvement of all six zones [10]. The scores for all six zones per chest radiographic study were summed to yield a cumulative chest radiographic score ranging from 0 to 24 depending on the involvement of the lung parenchyma. The scores were recorded at initial presentation and at the peak of disease activity.

The serial frontal chest radiographs obtained during treatment were also reviewed to examine the extent of radiographic deterioration during disease progression. Disease progression was classified as described by Wong et al. [8], with minor modifications to the definitions of type 2 and type 3 disease progression. Type 2 disease progression was defined as static radiographic changes with no discernible radiographic peak or change in overall mean lung involvement of less than 25%. Type 3 disease progression was defined as fluctuating radiographic changes with at least two radiographic peaks separated by a period of mild remission, with remission defined as a level of mean lung parenchyma involvement that differed from the peak level by more than 25%. Type 1 progression (i.e., initial radiographic deterioration followed by improvement) and type 4 progression (i.e., progressive radiographic deterioration) were defined as previously described [8].

Medical charts were reviewed to obtain information regarding comorbidities, demographic characteristics, symptoms, duration of hospitalization, admission to the ICU, initiation and duration of mechanical ventilation, and death. One patient with a prior diagnosis of lung fibrosis was also included in the study, although this fact was withheld from the reviewers reviewing the chest radiographs. All patients who recovered were contacted within 1 week and were asked to report any additional symptoms, additional medical treatment, rehospitalization, and current status.

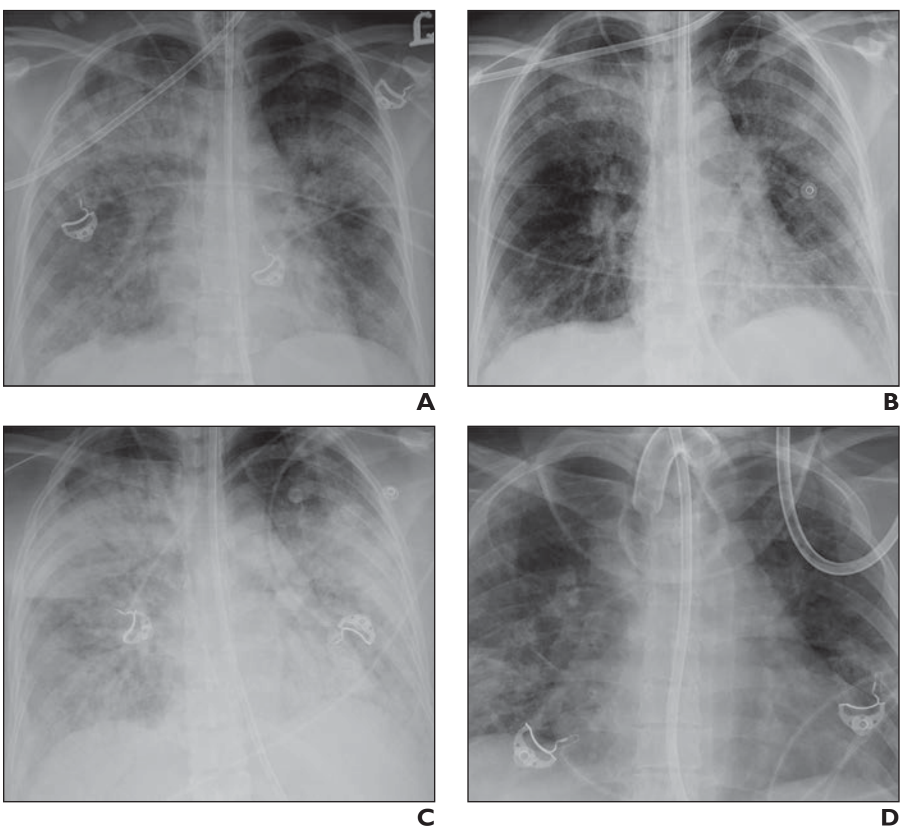

Fig. 4—32-year-old woman with Middle East respiratory syndrome coronavirus. Serial radiographs show type 3 radiographic deterioration pattern.
A, Frontal chest radiograph obtained on day 4 after admission to ICU shows right upper and middle zone consolidation along with ground-glass opacities in left middle zone; chest radiographic score is 7.
B, Subsequent follow-up chest radiograph obtained on day 7 after admission to ICU shows significant improvement but remaining bilateral ill-defined ground-glass opacities; chest radiographic score is 2.
C, Follow-up frontal chest radiograph obtained on day 10 after admission to ICU shows recurrence of bilateral significant airspace disease; chest radiographic score is 13.
D, Follow-up frontal chest radiograph obtained on day 19 after admission to ICU shows almost total improvement but bilateral basal ill-defined ground-glass opacities are still present; chest radiographic score is 1. Patient made complete recovery.

Statistical Analyses

The 55 subjects were divided into two groups according to final outcome. The deceased group included 19 patients who died and the recovered group included 36 patients who recovered. The mean percentage lung involvement at initial presentation and at the time of peak activity, the pattern of disease progression on chest radiographs (types 1–4), and the presence or absence of other chest radiographic parameters (ground-glass, patchy, nodular, or confluent nodular opacities; areas of consolidation; linear airspace opacity; cavitation plus pleural effusion; and pneumothorax) were compared between the two groups. The chi-square test was used to compare categoric data, and the Student *t* test was used to compare normally distributed continuous variables. The Mann-Whitney *U* test was used to compare nonnormally distributed continuous variables. Kolmogorov-Smirnov tests were performed to check normal distribution between the groups for continuous variables. Demographic characteristics, chest radiographic scores, comorbidities, and platelet and absolute lymphocyte counts were also compared between groups. A Kaplan-Meier survival curve analysis was performed according to the number of days on mechanical ventilation. Quantitative variables were expressed as the mean ± SD or as the median and range, and qualitative variables were expressed as the frequency and percentage.

TABLE 1: Radiographic Findings in 55 Patients Infected With the Middle East Respiratory Syndrome Coronavirus (MERS-CoV)

Radiographic Findings	No. (%) of Patients			p
	Deceased Group ($n = 19$)	Recovered Group ($n = 36$)	Total	
Lung zones involved at initial presentation				
Right upper zone	4 (21.1)	5 (13.9)	9 (16.4)	0.5
Right middle zone	6 (31.6)	8 (22.2)	14 (25.5)	0.45
Right lower zone	11 (57.9)	13 (36.1)	24 (43.6)	0.12
Left upper zone	2 (10.5)	3 (8.3)	5 (9.1)	0.79
Left middle zone	8 (42.1)	8 (22.2)	16 (29.1)	0.12
Left lower zone	6 (31.6)	8 (22.2)	14 (25.5)	0.45
Lung zones involved at time of peak radiographic deterioration				
Right upper zone	11 (57.9)	12 (33.3)	24 (43.6)	0.09
Right middle zone	19 (100)	16 (44.4)	35 (63.6)	0.001
Right lower zone	19 (100)	21 (58.3)	40 (72.7)	0.001
Left upper zone	9 (47.4)	7 (19.4)	16 (29.1)	0.03
Left middle zone	18 (94.7)	19 (52.8)	37 (67.3)	0.002
Left lower zone	15 (78.9)	20 (55.6)	35 (63.6)	0.09
Abnormal findings on chest radiographs				
Ground-glass opacity	16 (84.2)	20 (55.6)	36 (65.5)	0.03
Consolidation	3 (15.8)	7 (19.4)	10 (18.2)	0.74
Patchy consolidation	5 (26.3)	5 (13.9)	10 (18.2)	0.26
Nodular areas of opacity	2 (10.5)	3 (8.3)	5 (9.1)	0.8
Irregular linear airspace disease	2 (10.5)	3 (8.3)	5 (9.1)	0.8
Confluent consolidation	7 (36.8)	9 (25)	16 (29.1)	0.36
Air bronchogram	2 (10.5)	4 (11.1)	6 (10.9)	0.95
Multicentric cavitation	1 (5.3)	0 (0)	1 (1.8)	0.16
Pleural effusion	12 (63.2)	5 (13.9)	17 (30.9)	0.001
Pneumothorax	9 (47.4)	0 (0)	9 (16.4)	0.001
Normal findings on chest radiographs	0 (0)	9 (25)	9 (16.4)	0.02

Multivariate logistic regression analysis was performed using significant and important variables identified by univariate analysis. A p value (two-tailed) of < 0.05 was considered statistically significant. All statistical analyses were performed using SPSS software (version 21.0, IBM).

Results

Clinical Presentation and Appearance of Abnormalities

The 55 patients underwent a total of 581 chest radiographic examinations. The indications for chest radiography were dyspnea or findings indicative of pneumonia on auscultation. The chest radiographic findings were considered abnormal in 46 of 55 (83%) patients. The radiologic findings are summarized in Table 1. The most frequently observed type of opacity was ground-glass (36/55, 66%) (Fig. 1) followed by consolidation (10/55, 18%). Both ground-glass opacity and consolidation were noted in 9 of 55 (16%) patients. Consolidations appeared patchy (10/55, 18%) or confluent (16/55, 29%) or as rounded nodular areas of opacity (5/55, 9%). Air bronchogram was noted in 6 of 55 (11%) patients. Irregular linear airspace disease was noted in 5 of 55 (9%) patients and multicentric cavitation was noted in one patient (1/55, 2%) (Fig. 2).

Distribution of Abnormalities

Initial lung involvement (Table 1) was noted in the right lower (24/55, 44% of cases) and left middle (16/55, 29%) zones. The radiographic distribution at the time of peak radiographic deterioration (Table 1) was more significant in deceased patients who showed a higher incidence of right lower zone (19/19, 100%; $p = 0.001$), right middle zone (19/19, 100%; $p = 0.001$), and left middle zone (18/19, 95%; $p = 0.002$) involvement. Peripheral distribution was a predominant feature (32/55, 58%), which was followed by central distribution (14/55, 25%) and combined central and peripheral distribution (8/55, 15%). Unifocal involvement (38/55, 69%) was more common than multifocal involvement (17/55, 31%). At initial presentation, the median number of lung zones involved was two (range, 1–5 zones) in patients who died and one (range, 0–4 zones) in patients who recovered.

Duration of Hospital Stay and Disease Course

The duration of the hospital stay (from the time of admission) ranged from 1 to 34 days (mean, 12.5 ± 8.6 days). Of the 55 subjects examined, 30 (55%) were admitted to the ICU for mechanical ventilation, treatment of acute respiratory distress syndrome (ARDS), or both. During the later stage of the disease, 17 of 55 (31%) patients developed pleural effusion (Fig. 3) and 9 of 55 (16%) developed pneumothorax. All nine of the patients who developed pneumothorax were intubated. The incidence of pleural effusion (12/19, 63%; $p = 0.001$) and the incidence of pneumothorax (9/19, 47%; $p = 0.001$) were higher in the deceased group than in the recovered group (Table 1). The mean number of days from symptom onset to the day of death or recovery was 12 ± 8.5 for the deceased group and 12.6 ± 8.9 for the recovered group (Table 2).

Superinfection

Of the 30 patients admitted to the ICU, nine (9/30, 30%) developed superinfection; bacteria were isolated from multiple nasopharyngeal aspirates. None of the patients underwent bronchoscopy or bronchial lavage. The culture results were as follows: *Pseudomonas aeruginosa* ($n = 4$, 44%), *P. aeruginosa* and *Klebsiella* species ($n = 1$, 11%), *Stenotrophomonas maltophilia* and *Pseudomonas* species ($n = 1$, 11%), *P. aeruginosa* and methicillin-resistant *Staphylococcus aureus* ($n = 1$, 11%), *P. aeruginosa* and *Providencia stuartii* ($n = 1$, 11%), and methicillin-resistant *S. aureus* ($n = 1$, 11%). Six of the nine patients died, and three were treated successfully and made a full recovery.

TABLE 2: Comparison of Imaging and Clinical Interval Variables and Outcome in 55 Patients Infected With the Middle East Respiratory Syndrome Coronavirus

Variable	Deceased Group ($n = 19$)	Recovered Group ($n = 36$)	p
Imaging variables			
No. of lung zones involved at initial presentation, median (range)	2 (1–5)	1 (0–4)	0.02
Chest radiographic score at initial presentation, mean ± SD	1.4 ± 0.8	1.9 ± 1.3	0.35
Chest radiographic score at time of peak radiographic deterioration, mean ± SD	13 ± 2.6	5.8 ± 5.6	0.001
No. of chest radiographic examinations, mean ± SD	13 ± 8	9 ± 10	0.11
Clinical variables			
Age (y), mean ± SD	54.5 ± 17	43 ± 15	0.01
Mechanical ventilation (d), mean ± SD	11 ± 8	6 ± 9	0.03
Platelet count (× 10^9 cells/L), median (range)	120 (34–349)	210 (54–404)	0.17
Absolute lymphocyte count (× 10^9 cells/L), median (range)	9 (4–51.6)	24 (4–83)	0.01
No. of comorbidities, mean ± SD	2.26 ± 1.4	0.5 ± 0.70	0.001
No. of days between disease onset and death or recovery, mean ± SD	12 ± 8.5	12.6 ± 8.9	0.88

TABLE 3: Demographic and Clinical Characteristics of Health Care Workers (HCWs) Infected With the Middle East Respiratory Syndrome Coronavirus (MERS-CoV) and of MERS-CoV-Infected Patients

Variable	HCWs ($n = 22$)	Patients ($n = 33$)	p
Age (y), mean ± SD	34 ± 7	54 ± 16	0.001
No. of comorbidities, mean ± SD	0.17 ± 0.65	1.90 ± 1.27	0.001
Absolute lymphocyte count (× 10^9 cells/L), mean ± SD	25.8 ± 8	20.5 ± 17.5	0.001
Radiographic progression, no. (%) of patients			
Type 1	3 (13.6)	1 (3)	0.14
Type 2	9 (40.9)	11 (33.3)	0.5
Type 3	1 (4.5)	6 (18.2)	0.14
Type 4	1 (4.5)	13 (39.4)	0.004
Chest radiographic score at initial presentation, mean ± SD	0.71 ± 0.80	1.52 ± 1.3	0.009
Chest radiographic score at time of peak radiographic deterioration, mean ± SD	4 ± 5	11 ± 4.4	0.001
No. (%) of subjects who died	1 (4.5)	18 (54.5)	0.001

Progressive Deterioration on Chest Radiographs and Its Relationship to Final Outcome

The chest radiographic score of the deceased patients (Table 2) increased significantly from 1.4 ± 0.8 at initial presentation to 13 ± 2.6 at the time of peak radiographic deterioration ($p = 0.001$). The chest radiographic score at the time of peak radiographic deterioration was significantly higher ($p = 0.001$) for the patient group than for the HCW group (Table 3). Details of the chest radiographic deterioration pattern based on the analysis of serial chest radiographs from the patient group and HCW group are presented in Table 3. Mortality was highest in those with type 4 progression (12 deaths [12/19, 63%] $p = 0.001$; Fig. 1), followed by type 3 progression (four deaths [4/19, 21%] $p = 0.18$; Fig. 4) and type 2 progression (three deaths [3/19, 16%] $p = 0.01$; Table 4). Of the 30 patients who were intubated in the ICU, 19 died and 11 survived. Of the 19 subjects who died, 18 were in the patient group (18/33, 55%) and one was in the HCW group (1/22, 5%) (Table 3). The three subjects who died of type 2 disease progression were 20, 79, and 80 years old, and each had serious comorbidities (a right atrial tumor, acute cholecystitis, and lung fibrosis, respectively). The patient with lung fibrosis died despite the fact that the areas of consolidation were limited to the right lower lobe.

Comorbidities

The number of comorbidities in the deceased group was higher (2.26 ± 1.4) than that in the recovered group (0.5 ± 0.7). Overall, 24 (44%) patients had no comorbidities, 13 had one comorbidity (24%), nine (16%) had two, and nine (16%) had three or more. Comorbidities included diabetes mellitus ($n = 11$), hypertension ($n = 11$), ischemic heart disease ($n = 7$), end-stage renal disease ($n = 4$), chronic obstructive lung disease ($n = 3$), leukemia ($n = 3$), smoking ($n = 3$), asthma ($n = 2$), cardiac bypass surgery ($n = 2$), obesity ($n = 2$), multiple myeloma ($n = 2$), pulmonary artery hypertension ($n = 2$), pulmonary embolism ($n = 2$), liver cirrhosis ($n = 2$), lymphoma ($n = 2$), brain tumor ($n = 1$), postoperative complications ($n = 1$), congestive heart failure ($n = 1$), lung fibrosis ($n = 1$), acute cholecystitis ($n = 1$), unstable gait ($n = 1$), cardiac mass ($n = 1$), carcinoma of the breast ($n = 1$), hepatitis B ($n = 1$), metastases to the brain ($n = 1$), carcinoma of the ovary ($n = 1$), and mild renal impairment due to diabetes mellitus ($n = 1$). A 20-year-old woman with an irregular right atrial cardiac mass on chest CT died before a planned biopsy. The number of comorbidities in the patient group was significantly higher than that in the HCW group (1.90 ± 1.27 vs 0.17 ± 0.65, respectively; $p = 0.001$) (Table 3).

Predictors of Final Outcome

A Kaplan-Meier analysis (Fig. 5) revealed a 15-day median survival rate (95% CI, 4–26 days). Logistic regression analysis adjusted for significant variables identified by univariate analysis identified the chest radiographic score as an independent predictor of mortality (OR, 1.38; 95% CI, 1.07–1.77; $p = 0.01$) (Table 5).

Pleural effusion ($p = 0.001$), pneumothorax ($p = 0.001$), a low absolute lymphocyte count ($p = 0.001$), and type 3 ($p = 0.18$) or type 4 ($p = 0.001$) radiographic progression were noted in a significantly higher number of deceased patients than recovered patients (Tables 1, 2, and 4); thus, these characteristics are ominous signs of an impending fatal outcome.

The patient group ($n = 33$) (Table 3) had significantly more comorbidities ($p = 0.001$), a higher average age ($p = 0.001$), higher chest radiographic scores (initial, $p = 0.009$; peak, $p = 0.001$), and a lower absolute lymphocyte count ($p = 0.001$) than the HCW group

TABLE 4: Relationship Between Type of Progression and Final Outcome in 55 Patients Infected With the Middle East Respiratory Syndrome Coronavirus

Variable	Deceased Group ($n = 19$)	Recovered Group ($n = 36$)	p
Age (y), mean ± SD	54.5 ± 17	43 ± 14.5	0.01
Radiographic progression, no. (%) of patients			
Type 1	0 (0)	4 (11.1)	0.13
Type 2	3 (15.8)	18 (50)	0.01
Type 3	4 (21.1)	3 (8.3)	0.18
Type 4	12 (63.2)	2 (5.6)	0.001

TABLE 5: Predictors of Mortality in 55 Patients Infected With the Middle East Respiratory Syndrome Coronavirus

Variable	Adjusted Odds Ratio (OR)	95% CI	p
Age	0.99	0.94–1.05	0.83
Chest radiographic score	1.38	1.07–1.77	0.01
Absolute lymphocyte count	1	0.92–1.08	0.96
No. of comorbidities	0.79	0.41–1.50	0.47
Congestive heart failure	8.41	0.45–158.0	0.16
Hypertension	0.47	0.03–8.45	0.61
Diabetes mellitus	24.9	0.99–621.0	0.05

Note—After adjustment for significant variables in multivariate logistic regression analysis showed that chest radiographic score is an independent predictor of mortality (OR, 1.38; 95% CI, 1.07–1.77; $p = 0.01$).

($n = 22$). On the other hand, the chest radiographic score (mean, 4 ± 5; $p = 0.001$) and the incidence of type 4 radiographic progression (1/22, 5%; $p = 0.001$) were lower in the younger HCWs (34 ± 7 years) (Table 3) who had few or no comorbidities (0.17 ± 0.65 per person). HCWs also had a higher absolute lymphocyte count ($p = 0.001$) and a better survival rate (21/22, 95%).

Discussion

MERS was identified relatively recently, and the coronavirus is thought to be the causative organism. The most common type of opacity observed in the current study was peripheral ground-glass (66%), followed by consolidation and a combination of both ground-glass opacity and consolidation. Irregular linear airspace disease and multicentric cavitation were rarely observed. In terms of distribution, right lower zone involvement was the most frequent (73%) at the time of peak radiographic deterioration and was more significant in deceased patients; deceased patients showed a higher incidence of right lower zone (19/19, 100%), right middle zone (19/19, 100%), and left middle zone (18/19, 95%) involvement than patients who recovered. The chest radiographic score was an independent predictor of mortality. Radiographic findings of pleural effusion ($p = 0.004$), pneumothorax ($p = 0.001$), a high chest radiographic score (13 ± 2.6, $p = 0.001$), and a type 4 radiographic deterioration pattern ($p = 0.001$) were the major causes of high mortality rates, particularly when associated with other clinical factors such as age and preexisting comorbidities. Mortality rates were lower for HCWs who were significantly younger, had significantly fewer comorbidities, had a lower incidence of type 4 radiographic deterioration, and had a lower peak chest radiographic score than patients.

At our institution, patients presenting with fever and symptoms suggestive of respiratory illness (i.e., cough and shortness of breath) are carefully monitored for MERS-CoV infection. Nasopharyngeal swabs from these patients are immediately tested by RT-PCR to confirm or rule out the MERS-CoV. Chest radiographs are also obtained at initial presentation. In the current study, the group of patients presenting with dyspnea and showing peripheral ground-glass opacities on chest radiographs were triaged and admitted to a specialized ward for treatment, which was referred to as "corona fast-track." Other patients remained in isolation under close observation. Because this study is retrospective, there is no scoring system for triaging patients with MERS-CoV. However, the results of the current study suggest that patients should be actively managed as soon as possible using age, number of comorbidities, and chest radiographic score at peak radiographic deterioration to determine risk; the deceased patients in our study had the following characteristics: age of 54.5 ± 17 years, 2.26 ± 1.4 comorbidities, and a chest radiographic score at peak radiographic deterioration of 13 ± 2.6.

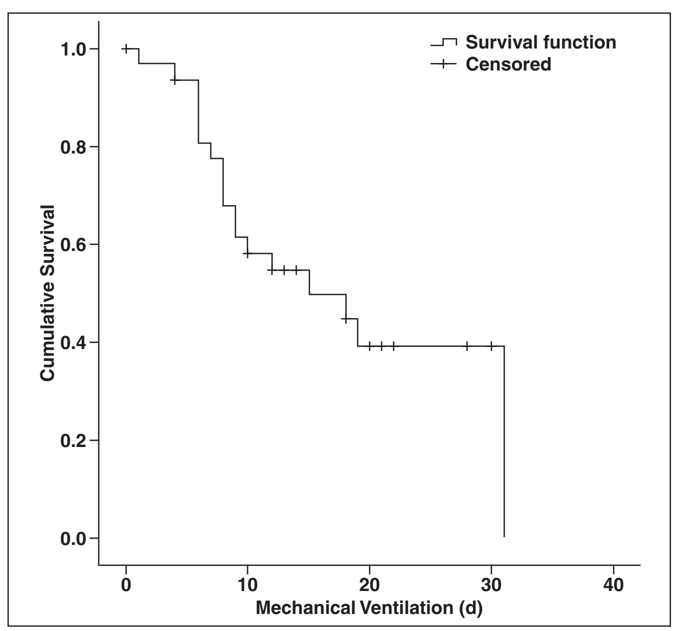

Fig. 5—Kaplan-Meier analysis reveals survival time of 55 patients infected with Middle East respiratory syndrome coronavirus. Median survival of study group was 15 days (95% CI, 4–26 days).

Pleural effusion in conjunction with other risk factors may be considered a significant predictor ($p = 0.001$ in the current cohort) of final outcome for patients with acute lung injury or ARDS who are admitted to the ICU [11]. Although a recruitment maneuver in the ICU can improve oxygenation in ARDS patients, this maneuver can be hindered by the presence of pleural effusion [11]. Similar problems were identified in the current cohort. Hasley et al. [12] reported that the presence of bilateral pleural effusions was an independent predictor of short-term mortality in patients with community-acquired pneumonia; however, in contrast to our experience, this relationship is absent in patients with severe acute respiratory syndrome (SARS) [8, 13].

Pneumothorax was another important predictor of an unfavorable outcome ($p = 0.001$) in the current study. Although the overall incidence of pneumothorax in MERS-CoV-infected patients (9/30 ICU patients, 30%) on mechanical ventilation was lower than that in SARS patients (12–34%) [14–16], a high percentage of deceased patients (9/19, 47%; $p = 0.001$) had this complication. The incidence of barotrauma in patients with acute lung injury or ARDS varies widely; recent studies report rates of 5–15% [17, 18]. Pneumothorax may be considered a sign of deteriorating respiratory function [19] in mechanically ventilated patients, as seen in the current cohort.

Superinfection is another complication that affects final outcome. In the current cohort, 9 of 30 (30%) patients admitted to the ICU for mechanical ventilation had secondary infections. A previous study reported concurrent bacterial infection in 29% of patients who died in an influenza pandemic; most of the isolated pathogens were typical of community-acquired pneumonia [20]. The initial chest radiographs obtained of our study group suggested that none of the subjects had a similar infection. However, progression from a low to a high chest radiographic score (from 1.4 ± 0.8 to 13 ± 2.6 in the deceased group and from 1.9 ± 1.3 to 5.8 ± 5.6 in the recovered group) may indicate either a severe viral infection or a high probability of superinfection. Experience of secondary superinfection, which results in considerable worsening of lung infections in MERS-CoV-infected patients (often culminating in ARDS), supports a policy of early antibiotic administration to treat bacterial pneumonia [5].

Peripheral ground-glass opacities on initial chest radiographs were indicative of MERS-CoV. Similar radiographic features, coupled with pleural effusions, may suggest bacterial, mycobacterial, and fungal pneumonias or Hantavirus infection [21]. The H1N1, SARS, and Cytomegalovirus viruses may cause homogeneous or patchy areas of peripheral ground-glass opacity that consolidate and rapidly progress to confluence, albeit rarely accompanied by pleural effusion [22–24]. Comparable presentations with occasional pleural effusion may be observed in patients with atypical pneumonia caused by *Chlamydia*, *Mycoplasma*, and *Legionella* species; patients with viruses that cause pneumonia in adults; patients with septic emboli; and patients with eosinophilic pneumonia [25–27]. Cytomegalovirus, herpesviruses, measles virus, and adenovirus mainly infect immunocompromised hosts [24, 25, 27]. These viral infections may present with overlapping radiographic findings [21]. The presence of characteristic clinical features, close contact with an established MERS-CoV-infected patient, and early peripheral ground-glass opacity on chest radiographs accompanied by lymphopenia should make clinicians highly suspicious of MERS-CoV infection.

This study has several limitations. First, preexisting disease, such as the lung fibrosis observed in one of our patients, may make it difficult to assess the extent of MERS-CoV infection because of overlapping radiographic findings. Second, the retrospective nature of the study may limit the power to identify clinical predictors. Third, visual estimation of the percentage of lung involvement is subjective and may not represent the actual involvement of the lung parenchyma; moreover, we did not compare frontal and lateral chest radiographs in all subjects. Fourth, we obtained no histopathologic evidence of disease in the patients who died.

In conclusion, the main radiographic feature observed on chest radiographs from MERS-CoV-infected patients was peripheral ground-glass opacity, with a preference for lower zone involvement in the majority of cases. Pleural effusion, pneumothorax, a higher chest radiographic score, and a high number of medical comorbidities in MERS-CoV-infected patients were indicative of a poor prognosis and high short-term mortality. However, younger HCWs with few or no comorbidities had a higher survival rate.

References

1. Zaki AM, Boheemen SV, Bestebroer TM, Osterhaus AD, Fouchier RA. Isolation of a novel coronavirus from a man with pneumonia in Saudi Arabia. *N Engl J Med* 2012; 367:1814–1820
2. Ministry of Health, Kingdom of Saudi Arabia, website. Statistics. www.moh.gov.sa/en/CCC/PressReleases/Pages/default.aspx. Accessed December 17, 2014
3. Hui DS, Memish ZA, Zumla A. Severe acute respiratory syndrome vs. the Middle East respiratory syndrome. *Curr Opin Pulm Med* 2014; 20:233–241
4. Al-Tawfiq JA, Assiri A, Memish ZA. Middle East respiratory syndrome novel corona MERS-CoV infection: epidemiology and outcome update. *Saudi Med J* 2013; 34:991–994
5. Assiri A, Al-Tawfiq JA, Al-Rabeeah AA, et al. Epidemiological, demographic, and clinical characteristics of 47 cases of Middle East respiratory syndrome coronavirus disease from Saudi Arabia: a descriptive study. *Lancet Infect Dis* 2013; 13:752–761
6. The WHO MERS-CoV Research Group. State of knowledge and data gaps of Middle East respiratory syndrome coronavirus (MERS-Cov) in humans. *PLoS Curr* 2013; 12:pii
7. Das KM, Lee EY, Enani MA, et al. CT correlation with outcomes in 15 patients with acute Middle East respiratory syndrome coronavirus. *AJR* 2015; 204:736–742
8. Wong KT, Antonio GE, Hui DS, et al. Severe acute respiratory syndrome: radiographic appearances and pattern of progression in 138 patients. *Radiology* 2003; 228:401–406
9. Hansell DM, Bankier AA, MacMahon H, McLoud TC, Müller NL, Remy J. Fleischner Society: glossary of terms for thoracic imaging. *Radiology* 2008; 246:697–722
10. Ooi GC, Daqing M. SARS: radiological features. *Respirology* 2003; 8(suppl):S15–S19
11. Lan CC, Hsu HH, Wu CP, Lee SC, Peng CK, Chang H. Influences of pleural effusion on respiratory mechanics, gas exchange, hemodynamics, and recruitment effects in acute respiratory distress syndrome. *J Surg Res* 2014; 186:346–353
12. Hasley PB, Albaum MN, Li YH, et al. Do pulmonary radiographic findings at presentation predict mortality in patients with community-acquired pneumonia? *Arch Intern Med* 1996; 156:2206–2212
13. Wong KT, Antonio GE, Hui DS, et al. Thin-section CT of severe acute respiratory syndrome: evaluation of 73 patients exposed to or with the disease. *Radiology* 2003; 228:395–400
14. Peiris JS, Chu CM, Cheng VC, et al. Clinical progression and viral load in a community outbreak of coronavirus-associated SARS pneumonia: a prospective study. *Lancet* 2003; 361:1767–1772
15. Lew TWK, Kwek TK, Tai D, et al. Acute respiratory distress syndrome in critically ill patients with severe acute respiratory syndrome. *JAMA* 2003; 290:374–380
16. Fowler RA, Lapinsky SE, Hallett D, et al.; To-

ronto SARS Critical Care Group. Critically ill patients with severe acute respiratory syndrome. *JAMA* 2003; 290:367–373

17. Eisner MD, Thompson BT, Schoenfeld D, Anzueto A, Matthay MA; Acute Respiratory Distress Syndrome Network. Airway pressures and early barotraumas in patients with acute lung injury and acute respiratory distress syndrome. *Am J Respir Crit Care Med* 2002; 165:978–982
18. [No authors listed]. Ventilation with lower tidal volumes as compared with traditional tidal volumes for acute lung injury and the acute respiratory distress syndrome: the Acute Respiratory Distress Syndrome Network. *N Engl J Med* 2000; 342:1301–1308
19. Kao HK, Wang JH, Sung CS, Huang YC, Lien TC. Pneumothorax and mortality in the mechanically ventilated SARS patients: a prospective clinical study. *Crit Care* 2005; 9:R440–R445
20. Centers for Disease Control and Prevention (CDC). Bacterial coinfections in lung tissue specimens from fatal cases of 2009 pandemic influenza A (H1N1): United States, May–August 2009. *MMWR Morb Mortal Wkly Rep* 2009; 58:1071–1074
21. Kim EA, Lee KS, Primack SL, et al. Viral pneumonias in adults: radiologic and pathologic findings. *RadioGraphics* 2002; 22:S137–S149
22. Agarwal PP, Cinti S, Kazerooni EA. Chest radiographic and CT findings in novel swine-origin influenza A (H1N1) virus (S-OIV) infection. *AJR* 2009; 193:1488–1493
23. Primack SL, Hartman TE, Ikezoe J, Akira M, Sakatani M, Müller NL. Acute interstitial pneumonia: radiographic and CT findings in nine patients. *Radiology* 1993; 188:817–820
24. Kang EY, Patz EF, Müller NL. Cytomegalovirus pneumonia in transplant patients: CT findings. *J Comput Assist Tomogr* 1996; 20:295–299
25. Ramsey PG, Fife KH, Hackman RC, Meyers JD, Corey L. Herpes simplex virus pneumonia: clinical, virologic, and pathologic features in 20 patients. *Ann Intern Med* 1982; 97:813–820
26. Tanaka H, Honma S, Yamagishi M, et al. Clinical features of measles pneumonia in adults: usefulness of computed tomography [in Japanese]. *Nihon Kyobu Shikkan Gakkai Zasshi* 1993; 31:1129–1133
27. Kawai T, Fujiwara T, Aoyama Y, et al. Diffuse interstitial fibrosing pneumonitis and adenovirus infection. *Chest* 1976; 69:692–694